Critical-Layer Structures and Mechanisms in Elastoinertial Turbulence

Ashwin Shekar,[1] Ryan M. McMullen,[2] Sung-Ning Wang,[1] Beverley J. McKeon,[2] and Michael D. Graham[1,*]
[1]*Department of Chemical and Biological Engineering, University of Wisconsin-Madison, Madison, Wisconsin 53706, USA*
[2]*Graduate Aerospace Laboratories, California Institute of Technology, Pasadena, California 91125, USA*

(Received 5 November 2018; published 29 March 2019)

Simulations of elastoinertial turbulence (EIT) of a polymer solution at low Reynolds number are shown to display localized polymer stretch fluctuations. These are very similar to structures arising from linear stability (Tollmien-Schlichting modes) and resolvent analyses, i.e., critical-layer structures localized where the mean fluid velocity equals the wave speed. Computations of self-sustained nonlinear Tollmien-Schlichting waves reveal that the critical layer exhibits stagnation points that generate sheets of large polymer stretch. These kinematics may be the genesis of similar structures in EIT.

DOI: 10.1103/PhysRevLett.122.124503

Turbulent drag reduction is an important and puzzling phenomenon in the non-Newtonian flow of complex fluids. Addition of polymers or micelle-forming surfactants to a liquid can lead to dramatic reductions in energy dissipation during turbulent flow while having a negligible effect on laminar flow [1].

In a Newtonian channel or pipe flow, transition to turbulence occurs by a so-called subcritical or "bypass" transition mechanism as the flow rate, measured nondimensionally by the Reynolds number, Re, increases: turbulence is initiated by finite-amplitude perturbations to the laminar flow profile, while the laminar flow remains linearly stable. While channel flow exhibits a two-dimensional linear instability leading to so-called Tollmien-Schlichting (TS) waves, the critical Reynolds number $\mathrm{Re} = 5772$ is much higher than that observed for transition, so these are not traditionally viewed as playing an important role in Newtonian transition.

For flowing polymer solutions under some conditions (low concentration, short polymer relaxation times), transition to turbulence occurs via the usual bypass mechanism. With further increase in Re, drag reduction sets in, and the flow eventually approaches the so-called maximum drag reduction (MDR) asymptote, an upper bound on the degree of drag reduction that is insensitive to the details of the fluid.

Under other conditions, flow transitions directly from laminar flow into the MDR regime, and can do so at a Reynolds number where the flow would remain laminar if Newtonian [2–5]. Recent experiments and simulations [6–8] suggest that turbulence in this regime has structure very different from Newtonian, denoting it as elastoinertial turbulence (EIT). Choueiri *et al.* [4] experimentally observed that at transitional Reynolds numbers and increasing polymer concentration, turbulence is first suppressed, leading to relaminarization, and then reinitiated with an EIT structure and a level of drag corresponding to MDR. Therefore, there are actually two distinct types of turbulence in polymer solutions, one that is suppressed by viscoelasticity, and one that is promoted.

The present work reports computations and analysis that elucidate the mechanisms underlying EIT. We show that EIT at low Re has highly localized polymer stress fluctuations. Surprisingly, these strongly resemble linear Tollmien-Schlichting modes as well as the most strongly amplified fluctuations from the laminar state. Furthermore, the kinematics of self-sustained nonlinear TS waves generate sheetlike structures in the stress field similar to those observed in EIT. The resemblance of structures at EIT to these Newtonian phenomena may shed light on the observed near universality of the MDR regime with regard to polymer properties.

Formulation.—We consider pressure-driven channel flow with constant mass flux. The x, y, and z axes are aligned with the streamwise (overall flow), wall-normal, and spanwise directions, respectively. Lengths are scaled by the half channel height l so the dimensionless channel height $L_y = 2$. The domain is periodic in x and z with periods L_x and L_z. Velocity $\boldsymbol{v}$ is scaled with the Newtonian laminar centerline velocity U, time t with l/U, and pressure p with ρU^2, where ρ is the fluid density. The polymer stress tensor $\boldsymbol{\tau}_p$ is related to the polymer conformation tensor $\boldsymbol{\alpha}$ (second moment of the probability distribution for the polymer end-to-end vector) through the FENE-P constitutive relation, which models each polymer molecule as a pair of beads connected by a nonlinear spring with maximum extensibility b. We solve the momentum, continuity, and FENE-P equations,

$$\frac{\partial \boldsymbol{v}}{\partial t} + \boldsymbol{v}\cdot\boldsymbol{\nabla}\boldsymbol{v} = -\boldsymbol{\nabla}p + \frac{\beta}{\mathrm{Re}}\boldsymbol{\nabla}^2\boldsymbol{v} + \frac{(1-\beta)}{\mathrm{ReWi}}(\boldsymbol{\nabla}\cdot\boldsymbol{\tau}_p), \quad (1)$$

$$\nabla \cdot \boldsymbol{v} = 0, \tag{2}$$

$$\boldsymbol{\tau}_p = \frac{\boldsymbol{\alpha}}{1 - \frac{\mathrm{tr}(\boldsymbol{\alpha})}{b}} - \boldsymbol{I}, \tag{3}$$

$$\frac{\partial \boldsymbol{\alpha}}{\partial t} + \boldsymbol{v} \cdot \nabla \boldsymbol{\alpha} - \boldsymbol{\alpha} \cdot \nabla \boldsymbol{v} - (\boldsymbol{\alpha} \cdot \nabla \boldsymbol{v})^T = \frac{-1}{\mathrm{Wi}} \boldsymbol{\tau}_p. \tag{4}$$

Here $\mathrm{Re} = \rho U l/(\eta_s + \eta_p)$, where η_s and η_p are the solvent and polymer contributions to the zero-shear rate viscosity. The viscosity ratio $\beta = \eta_s/(\eta_s + \eta_p)$; polymer concentration is proportional to $1 - \beta$. We fix $\beta = 0.97$ and $b = 6400$. The Weissenberg number $\mathrm{Wi} = \lambda U/l$, where λ is the polymer relaxation time, measures the ratio between the relaxation time for the polymer and the shear time scale for the flow. Below we report values of friction factor $f = (2\tau_w/\rho U^2)$, where τ_w is time- and area-averaged wall shear stress. This is a nondimensional measure of pressure drop or drag. Its value in laminar flow is denoted f_{lam}.

For the nonlinear direct numerical simulations (DNS) described below, a finite difference scheme and a fractional time step method are adopted for integrating the Navier-Stokes equation. Second-order Adams-Bashforth and Crank-Nicolson methods are used for convection and diffusion terms, respectively. The FENE-P equation is discretized using a high resolution central difference scheme [9–11]. No artificial diffusion is applied. For the three-dimensional (3D) simulations, $(L_x, L_y, L_z) = (10, 2, 5)$; these were chosen to match [6]. Typical resolution for the 3D runs at EIT is $(N_x, N_y, N_z) = (189, 150, 189)$. For the two-dimensional (2D) runs at $\mathrm{Re} = 3000$, $N_y = 302$ is used. For the linear analyses, Eqs. (2)–(4), linearized around the laminar solution and Fourier transformed in x, z, and t, are discretized in y with a Chebyshev pseudospectral method. Typically, about 200 Chebyshev polynomials are sufficient for the resolvent calculations, whereas as many as 400 are required for the TS eigenmode. The norm used in the resolvent calculations is the sum of the kinetic energy and a measure of the conformation tensor perturbation magnitude that is consistent with the non-Euclidean geometry of positive-definite tensors [12].

Nonlinear simulation results.—Figure 1 illustrates 3D DNS results for scaled friction factor $(f - f_{\mathrm{lam}})/f_{\mathrm{lam}}$ vs Weissenberg number Wi at $\mathrm{Re} = 1500$. At low but increasing Wi, the flow is turbulent, with f decreasing, indicating that the drag is reduced from the Newtonian value. In this regime, which we denote NT, the turbulence displays a streamwise vortex structure typical of Newtonian turbulence. With a further increase in Wi, however, $f - f_{\mathrm{lam}}$ drops to 0: the flow relaminarizes, as the NT regime loses existence. (At this Re and all Wi considered here, the laminar state is linearly stable.) At still higher Wi, the flow, if seeded with a sufficiently energetic initial condition, becomes turbulent again, with a very low value of $f - f_{\mathrm{lam}}$ (consistent with experimental observations of [4] in pipe flow) and a very different structure: i.e., a new kind of turbulence comes into existence. In this regime the flow structure corresponds to EIT as described by [6,8]; we further analyze this structure below. In short, as Wi increases from 0, the self-sustaining mechanism of Newtonian turbulence is weakened by viscoelasticity, resulting in loss of existence of the NT state. As Wi increases further, a new nonlinear self-sustaining (i.e., bypass transition) mechanism comes into play, resulting in EIT.

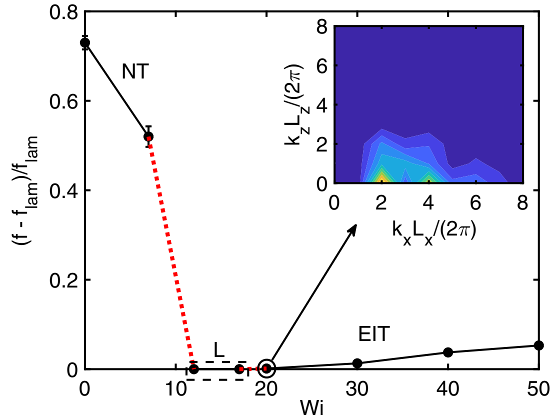

FIG. 1. Scaled friction factor vs Wi at $\mathrm{Re} = 1500$. Abbreviations NT, L, and EIT stand for Newtonian-like turbulence, laminar, and elastoinertial turbulence, respectively. In most cases, the error bars are smaller than the symbols. Red dotted lines indicate the intervals of Wi in which the NT solution loses existence and the EIT solution comes into existence, respectively, as Wi increases. The inset shows the spatial spectrum of the wall-normal velocity at $y = 0$ for $\mathrm{Wi} = 20$. Here, x- and z-wave numbers k_x and k_z are reported in scaled form, as $k_x L_x/2\pi$ and $k_z L_z/2\pi$. For the inset, low is blue, high is yellow.

We now focus on the flow structure in the EIT regime. The inset in Fig. 1 shows a spatial spectrum of the wall normal velocity at $y = 0$ (the channel centerplane), i.e., $|v_y(k_x, 0, k_z)|$. The centerplane is chosen because it yields the cleanest spectra. In the EIT regime, there is very strong spectral content when $k_z = 0$, indicating the importance of 2D mechanisms in the dynamics. Indeed, [8] reports that EIT can arise in 2D simulations. Figure 2(a) shows a slice at $z = 2.5$ of the fluctuating wall normal velocity, v_y', and fluctuating xx-component of the polymer conformation tensor, α_{xx}'. Observe that α_{xx}' is strongly localized near $y = \pm 0.7 - 0.8$. While tilted sheets of polymer stretch fluctuations have already been noted as characteristic of EIT [6], the strong localization has not been previously observed, perhaps because prior results have been at higher Re and Wi, i.e., further from the point at which EIT comes into existence. Figure 2(b) shows the dominant $(k_x L_x/2\pi, k_z L_z/2\pi) = (2, 0)$ component of the $\mathrm{Wi} = 20$ results, phase matched and averaged over many snapshots. Results for higher k_x are very similar, exhibiting strong localization of stress fluctuations in the same narrow bands, as well as velocity fluctuations that span the channel height.

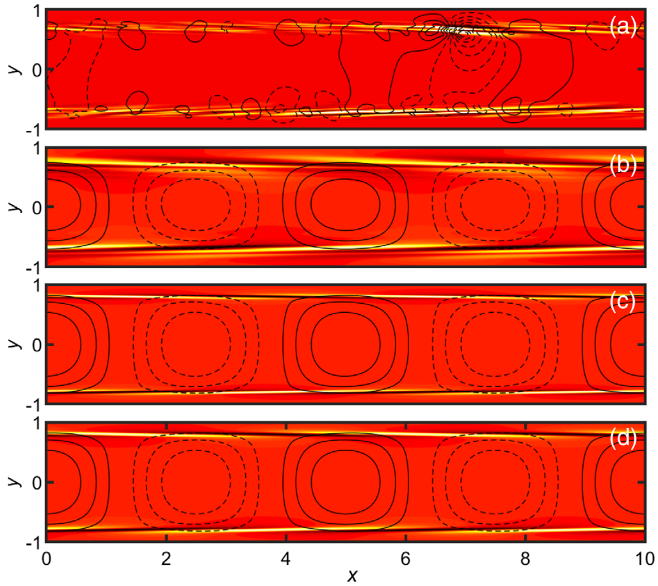

FIG. 2. (a) Snapshot of v_y' (line contours) and α_{xx}' (filled contours) from 3D nonlinear DNS at Re = 1500, Wi = 20, where $'$ denotes fluctuations. (b) Phase-matched average $(k_xL_x/2\pi, k_zL_z/2\pi) = (2,0)$ structures from 3D DNS. (c) Structure of the TS mode at Re = 1500, Wi = 20, and the same wave numbers as in (b). (d) Structure of the most strongly amplified resolvent mode at Re = 1500, Wi = 20, the same wave numbers as in (b), and $c = 0.37$. In all plots, contour levels are symmetric about 0. For v_y' dashed, negative; solid, positive. For α_{xx}' black, negative; red, zero; yellow, positive.

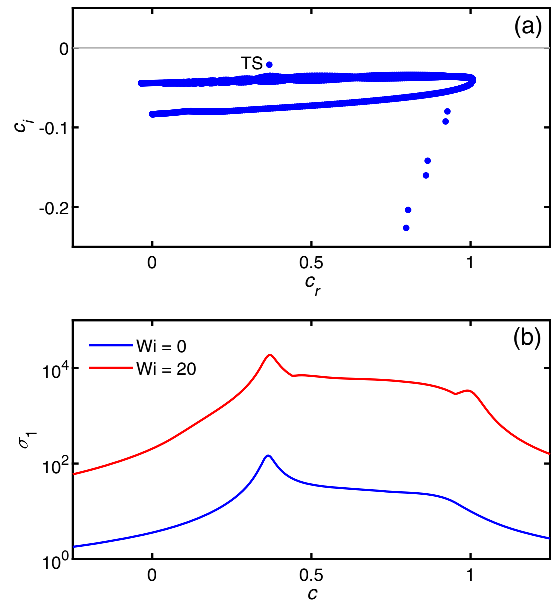

FIG. 3. Eigenvalue spectrum for $(k_xL_x/2\pi, k_zL_z/2\pi) = (2,0)$ with Wi = 20 and Re = 1500. The eigenvalue labeled TS corresponds to the TS mode. (b) Leading singular value of the resolvent operator for Wi = 0 and Wi = 20, plotted on a logarithmic scale.

Linear analyses.—To shed light on the origin of the highly localized large stress fluctuations, we now consider the evolution of infinitesimal perturbations to the laminar state with given wave numbers k_x, k_z. Two approaches are used. The first is classical linear stability analysis, in which solutions of the form $\phi(y)\exp[i(k_xx + k_zz - k_xct)]$ are sought, resulting in an eigenvalue problem for the complex wave speed c. If any $c_i > 0$, then the laminar state is linearly unstable—infinitesimal perturbations will grow exponentially. If all $c_i < 0$, the flow is linearly stable. The second approach is to determine the linear response of the laminar flow to external forcing with given real frequency ω using the resolvent operator (frequency-space transfer function) of the linearized equations [13,14]. In both analyses, the concept of *critical layers*, i.e., wall-normal positions where the streamwise velocity equals the wave speed of an eigenmode or resolvent mode, is important. While some recent studies suggest the importance of critical-layer mechanisms in viscoelastic shear flows [12,15–17], they do not make as direct a connection to EIT as we illustrate here.

Figure 3(a) shows the result of linear stability analysis (the eigenvalues c) for Wi = 20, $k_xL_x/2\pi = 2$, $k_z = 0$, the wave number corresponding to the dominant structures observed in the nonlinear simulations. All eigenvalues have $c_i < 0$: the laminar flow is linearly stable.

Of note is the mode labeled TS, the viscoelastic continuation of the classical Tollmien-Schlichting mode [18]. Viscoelasticity has only a weak effect on the TS eigenvalue, which changes from $c = 0.362 - 0.019i$ to $c = 0.368 - 0.022i$ between Wi = 0 and Wi = 20 [19]. Despite the small change in c, the conformation tensor disturbance depends very strongly on Wi; the peak value of α_{xx}' grows from 0 at Wi = 0 to $\sim 10^5$ times the peak value of v_x' at Wi = 20.

The structure of this eigenmode is shown for Wi = 20 in Fig. 2(c). In the Newtonian case, the disturbance velocity field is a train of spanwise-oriented vortices that span the entire channel; this structure is only weakly modified even at high Wi. The polymer stress disturbance behaves very differently: at Wi = 20 it consists of highly inclined sheets that are extremely localized around the critical layers $y = \pm 0.79$ for the TS wave speed of $c_r \approx 0.37$. Comparison with Figs. 2(a) and 2(b) shows a strong similarity between the eigenmode and the tilted sheetlike structures that are the hallmark of EIT, with the resemblance between the TS mode and the $(k_xL_x/2\pi, k_zL_z/2\pi) = (2,0)$ structure from the DNS in Fig. 2(b) being particularly striking. Specifically, note that for the TS mode, Fig. 2(c), v_y' and α_{xx}' are even and odd, respectively, with respect to $y = 0$, while in Fig. 2(b) and the corresponding results at higher wave numbers, these symmetries hold to a good approximation.

Despite the fact that the TS mode ultimately decays, the non-normal character of the linearized Navier-Stokes operator can lead to significant disturbance growth at short times or significant amplification of harmonic-in-time disturbances [13]. It is therefore possible for small disturbances to be sufficiently amplified that nonlinear effects become significant. We now quantify this amplification by computing the largest singular value σ_1 of the resolvent operator. Figure 3(b) shows results for $\mathrm{Wi} = 0$ and $\mathrm{Wi} = 20$ in the same range of (real) wave speeds $c = \omega/k_x$ depicted in Fig. 3(a). The amplification increases dramatically with Wi, with the values at $\mathrm{Wi} = 20$ being $\sim 10^2$ times those for $\mathrm{Wi} = 0$; this is consistent with the drastic increase in the conformation tensor disturbance amplitude already discussed for the TS mode. In both cases, the maximum amplification occurs for $c \approx 0.37$, which coincides with the wave speed for the TS mode, indicating that the most-amplified disturbance is closely linked to the TS wave. Figure 2(d) shows the leading resolvent mode, which is indeed almost identical to the TS eigenmode in Fig. 2(c). This result provides additional strong evidence that the structures observed in EIT are closely related to those in viscoelasticity-modified TS waves.

It was recently shown that viscoelastic pipe flow of an Oldroyd-B fluid ($b \to \infty$) can be linearly unstable to center-localized modes with wave speed $c_r \approx 1$ [20]. We estimate that for the present parameter values, this mode only becomes relevant for very high Wi. Furthermore, center-localized structures are not observed in the simulations of EIT, so we do not consider them relevant here.

Self-sustained viscoelastic Tollmien-Schlichting waves.— Here we elaborate on the potential connection between the TS-like structure and EIT, presenting results for nonlinear viscoelastic TS waves, i.e., self-sustained traveling wave solutions of the full nonlinear governing equations, illustrating the role of the critical-layer kinematics in generating localized sheetlike regions of high polymer stretching like those observed in EIT.

The strong peak in the EIT spectrum seen in Fig. 1 corresponds to a wavelength of 5, so here we report computations of nonlinear TS wave in a 2D domain with this length. The upper branch of this solution family is linearly stable in 2D at $\mathrm{Re} = 3000$ [21–23] and easily captured with DNS using the linear TS mode as the initial condition. In Newtonian flow, the solution family exists at this wavelength down to $\mathrm{Re} \approx 2800$. We continue the Newtonian solution at $\mathrm{Re} = 3000$ to the parameters of interest ($\beta = 0.97$ and $b = 6400$) at $\mathrm{Wi} = 0.1$, then increase Wi to study the effect of viscoelasticity. Hameduddin *et al.* [12] have computed nonlinear viscoelastic TS waves in the regime $\mathrm{Re} > 5772$ and noted the role the critical layer plays in polymer stretching at high Wi, but have not reported the observations described below.

On increasing Wi, the self-sustained nonlinear viscoelastic TS wave at $\mathrm{Re} = 3000$ develops sheets of high polymer stretch resembling near wall structures seen at EIT. Figure 4 illustrates this point with a plot of α_{xx} at $\mathrm{Wi} = 3$. The source of this stretching is closely tied to the critical-layer structure of the TS wave velocity field. Critical layers have long been known to exhibit a so-called Kelvin cat's-eye streamline structure [18]—indeed, the

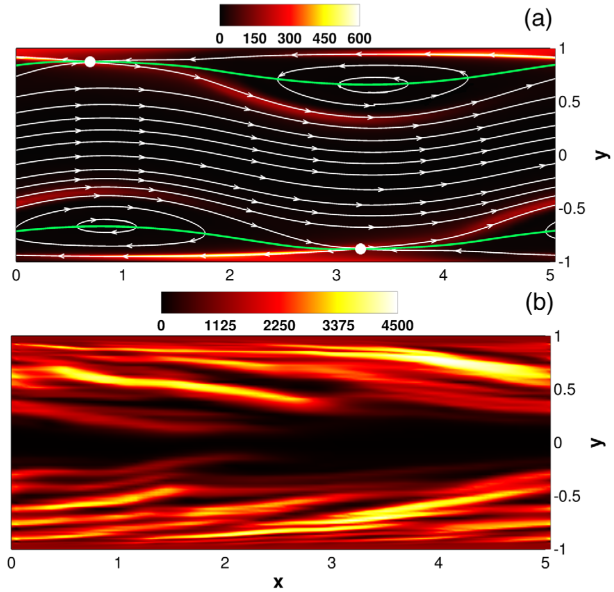

FIG. 4. (a) Structure of nonlinear self-sustaining TS wave at $\mathrm{Re} = 3000$, $\mathrm{Wi} = 3$. White streamlines, shown in a reference frame moving with the wave speed $c = 0.39$, are superimposed on color contours of α_{xx}. Green lines indicate the instantaneous critical-layer positions, and white dots indicate the locations of hyperbolic stagnation points. (b) Snapshot of α_{xx} contours from 2D EIT at $\mathrm{Re} = 3000$, $\mathrm{Wi} = 15$.

velocity fields for the flows shown in Figs. 2(c) and 2(d) display this feature. With regard to viscoelasticity, the cat's-eye structure is important because it contains hyperbolic stagnation points: polymers are strongly stretched as they approach such points and leave along their unstable manifolds. This phenomenon is clearly seen in Fig. 4(a); shown in white are streamlines in the reference frame traveling with the speed of the wave $c = 0.39$, and in green is the instantaneous critical-layer position, i.e., where $v_x = c$. A hyperbolic stagnation point (white dot) exists at $x = 3.22$, $y = -0.87$. The high polymer stretching follows the streamlines along the unstable directions associated with this point, giving rise to an arched sheetlike structure. By symmetry, identical structures exist in the top half of the channel. For comparison, Fig. 4(b) shows α_{xx} for 2D EIT at $\mathrm{Re} = 3000$, $\mathrm{Wi} = 15$. This takes the form of tilted sheets of high polymer stretch starting out at locations close to the walls, and in fact reasonably close to the positions $y = \pm 0.87$ of the stagnation points in the nonlinear TS wave at $\mathrm{Wi} = 3$. This similarity in structures suggests a role for TS wavelike critical-layer mechanisms at EIT. Indeed, these results suggest that the nonlinear TS wave solution branch may be directly connected in parameter space to EIT. We do not find this to be the case at $\mathrm{Re} = 3000$; the TS branch loses existence above $\mathrm{Wi} \approx 4$ and the EIT branch loses existence below $\mathrm{Wi} \approx 13$. Nevertheless, when using the EIT result at $\mathrm{Wi} = 13$ as the initial condition for a simulation at $\mathrm{Wi} = 12$, EIT persists transiently for hundreds of time units and the last remaining structure observed as the flow decays to laminar closely resembles Figs. 2(b)–2(d).

Conclusion.—Elastoinertial turbulence at low Re has strongly localized stress fluctuations, suggesting the importance of critical-layer mechanisms in its origin. These fluctuations strongly resemble the most slowly decaying structures from linear stability analysis, as well as the most strongly amplified disturbances as determined by resolvent analysis of the linearized equations. Furthermore, the Kelvin cat's-eye kinematics found in the critical-layer region of self-sustained nonlinear TS waves generate sheetlike structures in the stress field that resemble those observed in EIT. Taken together, these results suggest that, at least in the parameter range considered here, the bypass transition leading to EIT is mediated by nonlinear amplification and self-sustenance of perturbations that generate TS-wavelike flow structures.

This work was supported by (UW) NSF Grant No. CBET-1510291, AFOSR Grants No. FA9550-15-1-0062 and No. FA9550-18-1-0174, and ONR Grants No. N00014-18-1-2865 and (Caltech) No. N00014-17-1-3022.

A. S. and R. M. M. contributed equally to this work.

*mdgraham@wisc.edu

[1] P. S. Virk, H. S. Mickley, and K. A. Smith, J. Appl. Mech. **37**, 488 (1970).
[2] P. C. Forame, R. J. Hansen, and R. C. Little, AIChE J. **18**, 213 (1972).
[3] J. W. Hoyt, Nature (London) **270**, 508 (1977).
[4] G. H. Choueiri, J. M. Lopez, and B. Hof, Phys. Rev. Lett. **120**, 124501 (2018).
[5] B. Chandra, V. Shankar, and D. Das, J. Fluid Mech. **844**, 1052 (2018).
[6] D. Samanta, Y. Dubief, M. Holzner, C. Schäfer, A. N. Morozov, C. Wagner, and B. Hof, Proc. Natl. Acad. Sci. U.S.A. **110**, 10557 (2013).
[7] Y. Dubief, V. E. Terrapon, and J. Soria, Phys. Fluids **25**, 110817 (2013).
[8] S. Sid, V. E. Terrapon, and Y. Dubief, Phys. Rev. Fluids **3**, 011301 (2018).
[9] A. Kurganov and E. Tadmor, J. Comput. Phys. **160**, 241 (2000).
[10] T. Vaithianathan, A. Robert, J. G. Brasseur, and L. R. Collins, J. Non-Newtonian Fluid Mech. **140**, 3 (2006).
[11] V. Dallas, J. Vassilicos, and G. Hewitt, Phys. Rev. E **82**, 066303 (2010).
[12] I. Hameduddin, D. F. Gayme, and T. A. Zaki, J. Fluid Mech. **858**, 377 (2019).
[13] P. J. Schmid, Annu. Rev. Fluid Mech. **39**, 129 (2007).
[14] B. J. McKeon and A. S. Sharma, J. Fluid Mech. **658**, 336 (2010).
[15] J. Page and T. A. Zaki, J. Fluid Mech. **777**, 327 (2015).
[16] S. J. Lee and T. A. Zaki, J. Fluid Mech. **820**, 232 (2017).
[17] S. J. Haward, J. Page, T. A. Zaki, and A. Q. Shen, Phys. Rev. Fluids **3**, 091302 (2018).
[18] P. G. Drazin and W. H. Reid, *Hydrodynamic Stability*, Cambridge Mathematical Libraries, 2nd ed. (Cambridge University Press, Cambridge, England, 2004).
[19] M. Zhang, I. Lashgari, T. A. Zaki, and L. Brandt, J. Fluid Mech. **737**, 249 (2013).
[20] P. Garg, I. Chaudhary, M. Khalid, V. Shankar, and G. Subramanian, Phys. Rev. Lett. **121**, 024502 (2018).
[21] J. Jiménez, J. Fluid Mech. **218**, 265 (1990).
[22] F. Mellibovsky and A. Meseguer, J. Fluid Mech. **779**, R1 (2015).
[23] T. Herbert, in *Proceedings of the Fifth International Conference on Numerical Methods in Fluid Dynamics, Twente University, Enschede, 1976* (Springer, New York, 1979), pp. 235–240.